ELSEVIER

Physica B 323 (2002) 100–106

PHYSICA B

www.elsevier.com/locate/physb

Dispersive Raman spectra observed in graphite and single wall carbon nanotubes

R. Saito[a,*], A. Jorio[b], A.G. Souza Filho[b,e], A. Grueneis[a], M.A. Pimenta[f], G. Dresselhaus[c], M.S. Dresselhaus[b,d]

[a] *Department of Electronic-Engineering, University of Electronic-Communications, 1-5-1 Chofugaoka, Chofy 182-8585, Tokyo, Japan*
[b] *Department of Physics, Massachusetts Institute of Technology, Cambridge, MA 02139-4307, USA*
[c] *Francis Bitter Magnet Laboratory, Massachusetts Institute of Technology, Cambridge, MA 02139-4307, USA*
[d] *Department of Electrical Engineering and Computer Science, Massachusetts Institute of Technology, Cambridge, MA 02139-4307, USA*
[e] *Dept. de Física, Univ. Federal do Ceará, Fortaleza-CE 60455-760, Brazil*
[f] *Dept. de Física, Univ. Federal de Minas Gerais, Belo Horizonte-MG 30123-970, Brazil*

Abstract

The disorder-induced D-band and some other non-zone center Raman modes of graphite and single wall carbon nanotubes are assigned to phonon modes in their respective Brillouin zones. In disordered graphite, the weak, dispersive phonon modes, which have been known but never assigned so far, are well described by the double resonance Raman process. All weak Raman peaks observed for sp^2 carbons are useful for determining the phonon dispersion relations of graphite. In carbon nanotubes, all semiconducting nanotubes and some metallic nanotubes have van Hove singular k points for their electronic and phonon energy dispersion curves at the Γ point of the Brillouin zone. A corresponding Raman process is relevant to explain the observed D-band and intermediate frequency spectra.

PACS: 78.30.Na; 78.66.Tr; 63.22

Keywords: Carbon nanotubes; Raman spectroscopy; D-band; Double resonance; Dispersive phonon mode

1. Introduction

In disordered graphite, carbon nanotubes and sp^2 carbon materials, the disorder-induced Raman peak, known as the D-band, has been observed around 1350 cm^{-1} for laser excitation energy $E_{laser} = 2.41$ eV [1–3]. Characteristic features of the D-band are that (1) the peak frequency increases with increasing E_{laser} by 53 cm^{-1} eV^{-1}, and (2) the relative intensity of the D-band Raman peak to the zone center G-band peak around 1590 cm^{-1}, I_D/I_G, increases with increasing disorder and with decreasing crystallite size [4–6]. The origin of the D-band peaks is understood by a (1) double resonance, (2) one-phonon-emission, and (3) second-order Raman process in which one of the two scattering processes is an elastic scattering process due to a defect, and the other is a phonon emitting (or absorbing) inelastic scattering process [7–9]. Here the words second-order Raman are used in general to denote two scattering events occurring in a Raman process, and we explicitly show one-phonon or two-phonon processes for the

*Corresponding author. Fax: +81-424-43-5210.
E-mail address: rsaito@ee.uec.ac.jp (R. Saito).

0921-4526/02/$ - see front matter
PII: S0921-4526(02)00992-4

second-order Raman process. If the two scattering processes of an electron are phonon processes (two phonons, second-order Raman), sample disorder is not needed. Thus, the corresponding second harmonic G′ Raman phonon peaks around 2700 cm^{-1} are known to be intense, disorder-independent peaks. In double resonance Raman scattering, there exist the following four electronic processes: (1) photon absorption by creating an electron and a hole at $\mathbf{k}$, (2) the electron scattering from $\mathbf{k}$ to $\mathbf{k}+\mathbf{q}$, (3) the electron back scattering from $\mathbf{k}+\mathbf{q}$ to $\mathbf{k}$, and (4) photon emission by recombining the electron and the hole at $\mathbf{k}$. If there exist real electronic states both for the scattered electronic states $E_{\mathbf{k}+\mathbf{q}}$ and for the excited electronic states $E_{\mathbf{k}}$ at either the incident or the back scattered $\mathbf{k}$ states, the Raman intensity is doubly enhanced by the resonant factors [8,9]. This is the origin of the relatively strong enhancement of D-band Raman modes in sp^2 carbons. In this paper we discuss the origin of the D-band and other intermediate Raman modes of graphitic materials and single wall carbon nanotubes (SWNTs) on the basis of the double resonance process.

An important fact of the double resonance process is that the phonon q-vector is no longer around the center of the Brillouin zone (BZ), but corresponds to a general phonon mode in the BZ. Furthermore, by changing the laser excitation energy E_{laser}, the double resonance Raman peaks can shift along many phonon energy dispersion relations with different q-vectors. The resulting features in the Raman spectra have been known for many years as small, reproducible, and dispersive intermediate frequency Raman peaks [5,10–16]. Here we explain the relationship between the electron k-vector and the phonon q-vector to reproduce these peaks. As a result, almost all intermediate phonon modes are now assigned to specific branches on the phonon energy dispersion relations.

2. Double resonance condition for graphite

First we consider the resonant scattering of an electron with wave vector k by elastic or inelastic scattering vector q. The energy momentum conservation requires the following equations,

$$E(k+q) = E(k), \text{ or } E(k+q) = E(k) \pm \hbar\omega(q), \quad (1)$$

for elastic or inelastic scattering, respectively. The symbol $\pm$ corresponds to phonon absorption and emission, respectively. In the back scattering process from $k+q$ to k, the equations becomes, $E(k) = E(k+q)$ or $E(k) = E(k+q) \pm \hbar\omega(-q)$.

In graphite, the electronic energy dispersion is approximated by a linear dispersion relation around the K points at the corners of hexagonal BZ,

$$E = \pm\frac{\sqrt{3}\gamma_0 a}{2}|k|, \quad (2)$$

where $\gamma_0 = 2.89$ eV and $a = 0.246$ nm are the nearest neighbor tight-binding parameter and lattice constant, respectively [17]. The length of the wave vector, $|k|$, is measured from the K point. For the periodic boundary conditions, there are two inequivalent K and K′ points in the two dimensional (2D) BZ [17]. For a given energy E, the energy contours, $E = E(k)$, are two thick circles around the K and K′ points as shown in Fig. 1. When the energy increases, the circles are deformed to a triangle which connects three nearest neighbor M points to a K point (see Fig. 1), and this is known as the trigonal warping effect [18]. For laser energies smaller than 3 eV, the energy dispersion of the bonding and anti-bonding π bands is almost symmetric, and furthermore we can use the approximation that the contour is a circle.

Since the phonon energy is much smaller than the laser excitation energy, we can neglect the phonon energy to discuss inelastic electron scattering as a first approximation. In electron scattering from k to $k+q$ states on the same contour line $E = E(k)$, there are two possible scattering processes. One is the scattering within a circle and the other is from one circle to the other circle. Hereafter, we refer to the two cases, respectively, as intra-valley (K→K, K′→K′) and inter-valley (K→K′, K′→K) scattering. Intra-valley scattering requires relatively small q vectors compared with the size of the BZ, while inter-valley scattering requires relatively large q vectors. The corresponding phonon modes of intra-valley and inter-valley

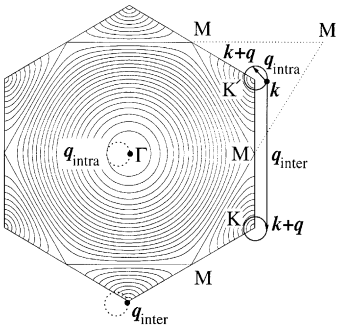

Fig. 1. Energy contours of 2D graphite. $E = E(k)$, and $E(k+q)$ are shown as thick solid circles around the hexagonal corners of the K or K′ points in the Brillouin zone of 2D graphite. When the energy increases, the circles are deformed to a triangle denoted by dotted line which connects three nearest neighbor M points to a K point. Dotted circles around the K and Γ points give all possible q_{inter} and q_{intra} vectors for a given k vector measured from Γ, shown near the upper-right K point.

scattering are related to the modes near the Γ and K points, respectively, when we measure the q vectors from the Γ point.

When we consider a k point on a circle $E = E(k)$, the end of all possible q vectors for intra-valley and inter-valley scattering lies, respectively, on the dotted circles, shown in Fig. 1, which touch the Γ and K points. The distance of the end points of the q vectors from the Γ or K points are expressed by

$$|q| = 2|k|\sin\theta, \tag{3}$$

where the angle θ is taken for $|\theta| < \pi/2$, and $\theta = 0$ corresponds to the largest q vector for each scattering case. The density of $|q|$ is singular at $|q| = 2|k|$, and thus the Raman spectra for phonons with $|q| = 2|k|$ will be enhanced. Further, the phonon $|q|$ wave vectors increase with increasing laser excitation energy. Using the fact that the phonon dispersion relation is symmetric around the Γ or K point, the phonon energy continuously changes along the various branches of the phonon dispersion relations by changing the laser energy. This is the physical origin of D-band phonon modes in sp^2 carbons. Another contribution to the intermediate Raman frequency features comes from phonons with $|q| = 0$. Although the density of phonon wave vectors in resonance $|q|$ is not singular at $|q| = 0$, the phonon dispersion relations around the symmetry points are flat (except for acoustic modes around the Γ point), and this gives rise to a singular phonon density of states (phonon DOS) [17].

The D-band phonon modes come from the second highest frequency phonon dispersion modes in sp^2 carbons by inter-valley phonon scattering. Since there are six phonon dispersion curves in 2D graphite, we can consider twelve possible double resonance peaks, which are generally dispersive depending on the slope of the phonon dispersion relation. Using the relation between $|q|$ and the laser energy, we can assign the experimental results for many dispersive phonons, and the results are summarized in Table 1. Tan et al. reported two dispersive relatively lower phonon frequency modes in graphite whiskers (GW) [11], which we assign to two of the three acoustic modes, the in-plane tangential (iTA) and longitudinal acoustic (LA) modes which are resonant through an intra-valley scattering process. The features around 1480 and 860 cm^{-1} are assigned for the first time to the inter-valley, in-plane tangential optical (iTO) and intra-valley, out-of-plane tangential optical (oTO) phonon branches, respectively. The broad weak signal around 1580 cm^{-1}, which is known as a background of the strong G-band peaks, is assigned to intra-valley scattering of the LO phonon dispersion branch. Furthermore, some non-dispersive modes can be assigned to $|q| = 0$ phonon modes.

In Fig. 2, we show the fitted phonon dispersion relations of graphite to the measured intermediate phonon frequencies. The original phonon dispersion relations that we used are based on inelastic neutron scattering experiments data [17] which are not so accurate in the higher frequency region. Since we do not get phonon frequency information near the M point from Raman spectra, we used lower frequency inelastic neutron scattering data [17], denoted by open circles, which are important to get good convergence for the fitting. The calculated frequencies and their dispersion slopes are consistent with each other and are in excellent agreement with the experimental results for all of these features. The details of the fitting procedure will be presented elsewhere [19].

Table 1
Assignment of intermediate phonon modes[a]

Mode assignment branch(process)	Theoretical value $\omega_{th}[\partial\omega/\partial E]$	Experimental observations $\omega_{exp}[\partial\omega/\partial E]$
oTA ($\Gamma, q = 2k$)	45[26]	—
iTA ($\Gamma, q = 2k$)	300[121]	288[129][6]
LA ($\Gamma, q = 2k$)	430[173]	453[216][6]
oTA (K, $q = 2k$)	500[−28]	—
oTO (K, $q = 2k$)	640[26]	—
	—	750[−147][5]
oTO ($\Gamma, q = 2k$)	850[−5]	865[13][3]
oTO ($\Gamma, q = 0$)	855[0]	860[0][5]
iTA (K, $q = 2k$)	900[−58]	820[−57][1], 865[−53][4], 1084[−74][2], 1094[−77][1]
iTA (K, $q = 0$)	1000[0]	970[129][5], 1060[0][5], 1081[22][4]
LA (K, $q = 2k$)	1250[−5]	—
LA/LO (K, $q = 0$)	1260[0]	—
LO (K, $q = 2k$)	1350[48]	1352[43][1], 1345[50][4], 1354[46][6]
iTO (K, $q = 2k$)	1450[−11]	1480[−83][1]
iTO (K, $q = 0$)	1490[0]	1500[−][2]
iTO ($\Gamma, q = 2k$)	1555[−20]	—
iTO/LO ($\Gamma, q = 0$)	1580[0]	1582[0][3]
LO ($\Gamma, q = 2k$)	1600[4]	1622[0][1], 1623[0][2], 1623[9][6]

[a] The first column shows the phonon dispersion mode (i = in-plane or o = out-of-plane, T = tangential or L = longitudinal, A = acoustic or O = optical, and Γ = intra-valley or K = inter-valley, $q = 0$ or $2k$). The second column shows the calculated phonon frequencies (for $E_{laser} = 2.41$ eV) and phonon frequency dispersions with laser energy $\partial\omega/\partial E$ (between brackets) for the Raman features predicted to appear in the Raman spectra of sp^2 carbons according to the double resonance theory. The third column correlates the predicted frequencies and dispersion with many Raman features experimentally observed in different sp^2 carbons, including (1) highly ordered pyrolytic graphite (HOPG) [14], (2) pyrolytic graphite (PG) [13], (3) single wall carbon nanotubes (SWNTs) [15], (4) ^{12}C ion implanted HOPG (C-HOPG) [12], (5) micro-crystalline graphite (MG) [5], and (6) graphite whiskers (GW) [11]. The frequencies are displayed in cm^{-1} and the frequency dispersions in cm^{-1} eV^{-1}.

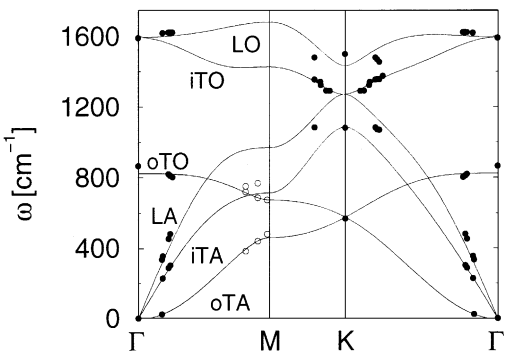

Fig. 2. Fitted graphite phonon dispersion relations to the intermediate frequency Raman peaks (solid circles). To get good convergence, we also use some inelastic neutron data, which are denoted by open circles.

In the double resonance phonon process, there are two resonant conditions: resonances with the incident and the scattered light, and thus a broad peak can be decomposed into two peaks, but it might be difficult in practice to decompose the broad experimental peaks into two peaks. However, when we measure both the Stokes and anti-Stokes peaks, the peak which comes from resonance with the incident photon should have the same energy for both the Stokes and anti-Stokes processes. Furthermore, the frequency separation of the scattered light resonance peak from the incident light resonance peak is the same for the Stokes and the anti-Stokes features. Thus, from the simultaneous measurement of the Stokes and anti-Stokes features, we can determine the slope of the phonon dispersion curve reliably. In preliminary measurements for the D-band of PPP-derived 2D graphite, a value of 58 cm^{-1} eV^{-1} was obtained [20], slightly higher than the previous value of 53 cm^{-1} eV^{-1}.

Elastic scattering provides another process to get one-phonon energy loss, and some electronic potential for defects is then needed for this elastic

scattering process. Since inter-valley elastic scattering requires relatively large q values, the corresponding scattering potential for an electron should be short range, smaller than the lattice constant $a = 0.246$ nm. Thus, a short range potential, such as a missing carbon atom or a pentagon–heptagon pair may be a candidate for giving rise to D-band light scattering.

3. D-band spectra of single wall carbon nanotubes

In the case of single wall carbon nanotubes (SWNTs), a resonance effect similar to that in sp^2 carbons is expected. In fact, Raman measurements of SWNT bundles [10,21–24], and isolated SWNTs [25–32] show a dispersive behavior by changing the laser energy. In particular, Alvarez et al. [15] reported three dispersive phonon modes around 850 cm^{-1} for SWNT bundles. One of the three is not so dispersive, and this mode can be assigned to intra-valley, TO phonon dispersion. However, the other two phonon modes have dispersive slopes that are too large to be explained by a single phonon emission second-order process. Thus, the remaining two dispersive modes are assigned to a two-phonon second-order process. The largest slope of the phonon dispersion relations is a longitudinal acoustic phonon mode near the Γ point (216 cm^{-1} eV^{-1}).

The dispersive nature of the D-band is explained by a double-resonance process. However, the dispersive D-band frequency and other intermediate phonon modes are given by different SWNTs which are resonant with different laser energies, taking into consideration that both the D-band frequency and the energy of the optical transitions in isolated SWNTs are dependent on the tube diameter. In SWNTs, the periodic boundary condition along the circumferential direction gives discrete k and q vectors which are expressed by the cutting lines in the 2D BZ (zone folding). In this case, the zone-folding of the K point is important to understand the double resonance process.

For (n,m) nanotubes, suppose that the K point is folded into the one dimensional (1D) BZ at the Y point and the distance of Y from the Γ point in the 1D BZ is given by [17],

$$\Gamma Y = \frac{m}{d_R}|\mathbf{K}_2|, \tag{4}$$

where $|\mathbf{K}_2|$ is the length of the 1D BZ (reciprocal lattice vector) and d_R is the greatest common divisor (gcd) of $(2m+n)$ and $(2n+m)$. Here d_R can be related to d, which is the gcd of n and m, by the relation

$$d_R = \begin{cases} d & \text{if } n-m \text{ is not a multiple of } 3d \\ 3d & \text{if } n-m \text{ is a multiple of } 3d. \end{cases} \tag{5}$$

In semiconducting nanotubes for which $n-m$ is not a multiple of 3, $d_R = d$ and thus m/d_R in Eq. (4) becomes an integer. This means that the K point is zone-folded into the Γ point of the 1D BZ for all semiconducting nanotubes. On the other hand, in metallic nanotubes, for which $n-m$ *is* a multiple of 3, there are two cases (metal-1 and metal-2) [17]. In metal-1, $d_R = d$ and thus the K point is zone folded into the Γ point of the 1D BZ, while in metal-2, $d_R = 3d$, and thus the K point is zone folded into $k = \pm|K_2|/3$.

Very recently Maultzsch et al. [33] discussed the double resonance effect of single wall nanotubes and concluded that only metal-2 SWNTs gave rise to D-band spectra. However, it is clear experimentally that both metal-1 and semiconducting nanotubes also show D-band spectra, from one isolated SWNT spectroscopy [27–29]. Since the resonant energy window of the Raman spectra for semiconducting and metallic SWNTs are different from each other, there is no possibility for observing metallic nanotubes in the semiconducting energy window for one isolated SWNT. This discrepancy between theory and experiment may come from the fact that the k vector which gives the van Hove singularity (VHS) in the electronic DOS, k_{VHS} is not always folded exactly to the Γ point of the 1D BZ. In fact, the k_{VHS} vectors for many (n,m) values which are resonant with a given laser energy exist homogeneously on an energy contour $E = E(k)$ in the 2D BZ. The corresponding locations of the folded k_{VHS} vectors in the 1D BZ are distributed homogeneously on the 1D BZ. Thus a double resonance process similar to that for graphite is expected for all nanotubes. Isolated SWNT micro Raman measurements show that the

distance of k_{VHS} from the K point in the 2D BZ is related to the D-band phonon wave vector for all SWNTs [29]. The application of the double resonance theory of graphite to SWNTs works well, too, for the results of Alvarez et al. [15].

It is noted that the VHS of the electronic DOS can give sufficient Raman intensity to observe the RBM and G-band phonon modes from one isolated SWNT [25,26,34]. In this case, both the singular enhancement of the first-order resonant condition and the VHS contribute to the strong Raman intensity that is observed. Furthermore, the D-band width from semiconducting nanotubes is small ($\sim 20\ cm^{-1}$) relative to that of graphite and some metallic nanotubes. This is due to the fact that some special k and q vectors are selected for making the D-band spectra. From these facts, another possibility is the case that the double resonance condition is not always necessary for observing D-band Raman spectra in metal-1 and semiconducting SWNTs. When both k and q vectors are near the Γ point of the 1D BZ, one-phonon emission, through a first-order process might contribute to the D-band intensity. The problem with the first-order process is that the phonon branch which corresponds to the D-band does not have Raman active symmetry. The Raman-active phonon modes instead come from the five cutting lines near the Γ points of the 2D BZ [35,36], and the cutting lines for phonons near the K point are not Raman active. However, defects may break the symmetry, or the symmetry selection rule may be broken under strong resonance conditions. Further investigation of this special case is needed in the future for each (n,m) value.

4. Conclusions

In conclusion, the double resonance theory for Raman spectroscopy reproduces the phonon dispersion relations of graphite. Stokes and anti-Stokes measurements of intermediate Raman frequencies determine the slopes of the phonon dispersion relations. D-band Raman spectra of SWNTs are explained by the van Hove singular k vectors which are folded into the 1D BZ for SWNTs.

Acknowledgements

The authors deeply thank Prof. Ping-Heng Tan for providing his unpublished data on the lower frequency dispersive phonon modes. R.S. acknowledges UFMG for support of the visit, a Grant-in-Aid (No. 13440091) from the Ministry of Education, Japan. A.J./A.G.S.F. acknowledge support from the Brazilian agencies CNPq/CAPES. The MIT authors acknowledge support under NSF Grants DMR 01-16042, INT 98-15744, and INT 00-00408.

References

[1] F. Tuinstra, J.L. Koenig, J. Chem. Phys. 53 (1970) 1126.
[2] M.S. Dresselhaus, P.C. Eklund, Adv. Phys. 49 (2000) 705.
[3] M.S. Dresselhaus et al., Carbon, 2002, Review article, in press.
[4] M.J. Matthews, et al., Phys. Rev. B 59 (1999) R6585.
[5] I. Pócsik, et al., J. Non-Crys. Solids 227-230 (1998) 1083.
[6] A.C. Ferrari, J. Robertson, Phys. Rev. B 61 (2000) 14095.
[7] O.V. Balagura, A.I. Ivanov, Opt. Spectrosc. (USSR) 62 (1987) 616.
[8] C. Thomsen, S. Reich, P.M. Rafailov, H. Jantoliak, Phys. Stat. Sol B, 2000.
[9] R. Saito, et al., Phys. Rev. Lett. 88 (2002) 027401.
[10] M.A. Pimenta, et al., Brazilian J. Phys. 30 (2000) 423.
[11] P.H. Tan, C.Y. Hu, J. Dong, W.C. Shen, B.F. Zhang, Phys. Rev. B 64 (2001) 214301.
[12] P.H. Tan, et al., Phys. Rev. B 58 (1998) 5435.
[13] Y. Kawashima, et al., Phys. Rev. B 52 (1995) 10053.
[14] Y. Kawashima, et al., Phys. Rev. B 59 (1999) 62.
[15] L. Alvarez, et al., Chem. Phys. Lett. 320 (2000) 441.
[16] P.H. Tang, et al., Appl. Phys. Lett. 75 (1999) 1524.
[17] R. Saito, G. Dresselhaus, M.S. Dresselhaus, Physical Properties of Carbon Nanotubes, Imperial College Press, London, 1998.
[18] R. Saito, G. Dresselhaus, M.S. Dresselhaus, Phys. Rev. B 61 (2000) 2981.
[19] A. Grueneis, R. Saito, Phys. Rev. B 65 (2002) 155405.
[20] L.G. Cançado et al. unpublished.
[21] A. Jorio, et al., Phys. Rev. Lett. 85 (2000) 2617.
[22] C. Fantini, et al., Phys. Rev. B 63 (2001) 161405.
[23] C. Thomsen, Phys. Rev. B 61 (2000) 4542.
[24] S.D.M. Brown, et al., Phys. Rev. B 61 (2000) 155414.
[25] A. Jorio, et al., Phys. Rev. Lett. 86 (2001) 1118.
[26] A. Jorio, et al., Phys. Rev. B 63 (2001) 245416.

[27] M.A. Pimenta, et al., Phys. Rev. B 64 (2001) 041 401.
[28] A.G. Souza Filho, et al., Chem. Phys. Lett. 354 (2002) 62.
[29] A.G. Souza Filho, et al., Phys. Rev. B 65 (2002) 085 417.
[30] G.S. Duesberg, et al., Phys. Rev. Lett. 85 (2000) 5436.
[31] J. Hwang, et al., Phys. Rev. B 62 (2000) R13 310.
[32] Z. Yu, L.E. Brus, J. Phys. Chem. B 105 (2001) 1123.
[33] J. Maultzsch, S. Reich, C. Thomsen, Phys. Rev. B 64 (2001) 121 407(R).
[34] A.G. Souza Filho, et al., Phys. Rev. B 63 (2001) 241 404.
[35] D. Kahn, J.P. Lu, Phys. Rev. B 60 (1999) 6535.
[36] R. Saito, et al., Phys. Rev. B 57 (1998) 4145.